Influence of resistivity on filamentary transport in the SOL of ASDEX Upgrade

D. Carralero [1], G. Birkenmeier[1], H.W. Müller[1], P. Manz [1], P. deMarne[1], S. Müller[2], U. Stroth[1], E. Wolfrum[1], and the ASDEX Upgrade team.

[1] *Max-Planck-Institut für Plasmaphysik, EURATOM Association, 85748 Garching, Germany.*

[2] *Center for Energy Research and Center for Momentum Transport and Flow Organization, University of California, San Diego, La Jolla, USA.*

Several widely accepted models [1, 2] describe the propagation of filaments in the scrape-off layer (SOL) as the result of the curvature drift and propose different regimes [3] depending on the parallel closure condition of the filament current circuit. In this sense, one of the key plasma parameters is the normalized collisionality, Λ [3]. Experiments on Alcator C-mod showed a dramatic change in the perpendicular to parallel transport balance when density is increased over 40% of the Greenwald limit [4], bringing the purely advective regime typically associated to the far SOL to the vicinity of the separatrix. A feedback mechanism relating lowered parallel transport with lower downstream temperature yielding even greater Λ, has been proposed as an explanation for this phenomenon [5]. In this work, we address this problem by analyzing the characteristics of density fluctuations and density radial transport in the outer midplane of ASDEX Upgrade (AUG) by means of reciprocating Langmuir probes for different values of line density -which is used as a proxy of viscosity [4]- in the range of $\bar{n}_{e,central}/n_{GW} \simeq [0.15, 0.6]$.

A number of L-mode discharges was carried out in AUG with constant magnetic parameters ($B_t = -2.5$ T, $q_{95} = 5.32$, $I_p = 800$ kA), constant heating (600 kW ECH) and edge line density ($\bar{n}_e$, measured by interferometry) increasing in a shot to shot basis in the $\bar{n}_e \in [0.75, 3] \cdot 10^{19}$ m^{-3} range. In order to achieve higher densities (up to $\bar{n}_e = 3.5 \cdot 10^{19}$ m^{-3}) without disrupting the plasma, an additional discharge is included in which the ECH power was increased up to 1 MW. Ion saturation current and floating potential in the SOL were measured with AUG's Midplane Manipulator (MEM), in which a 14-pin probe head was installed [6]. Density profiles were measured with the lithium beam diagnostic (LiB). During each discharge, the MEM was inserted to $R = 2.144$ m (42 mm in front of the limiter shadow) during four periods of some 100 ms. The separatrix was moved between plunges towards the wall in steps of 5 mm, yielding a range of probe distances of $\Delta R = R_{probe} - R_{sep} \in [15, 40]$ mm, roughly from the second density e-folding length to the limiter shadow. The data acquisition sampling rate was 2 MHz. In Figure 1 left, characteristic MEM position, R_{sep} and toroidal current (I_p) are displayed, along with $\bar{n}_e$

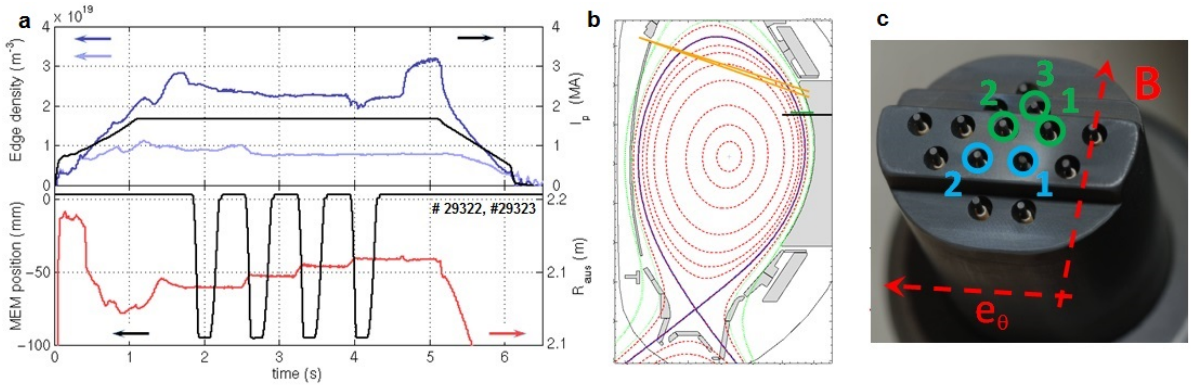

Figure 1: *Left, upper: dark/light curves display the $\bar{n}_e$ for discharges 29322/23. I_p displayed in black. Left lower, black/red curves indicate the MEM/separatrix position. Center, Diagnostic layout. Black line represents MEM position. Green line, LiB measurement region. Edge interferometer line is represented in orange. Right, 14 pin probehead. Green/blue circles indicate I_{sat}/V_f pins. Positive poloidal direction (red arrow) corresponds to electron diamagnetic direction.*

of discharges 29322 and 29323. As can be seen in the right diagram, pins are distributed in several radial levels (separation $L_r = 4$ mm) and poloidal positions ($L_\theta = 5.5$ mm), allowing for a complete description of the perpendicular structure of filaments.

Conditional average has been used to detect typical filaments: a filament event is defined as an ion saturation current fluctuation at pin 1 ($I_{sat,1}$) with an amplitude exceeding 2.5σ. For each event, signals from all five pins have been sampled over a window $T = \pm 0.5$ ms around the detection time. By averaging over all events in a given plunge, the typical filament signature for each pin is obtained. In Figure 2, left, a characteristic conditional averaging result is displayed.

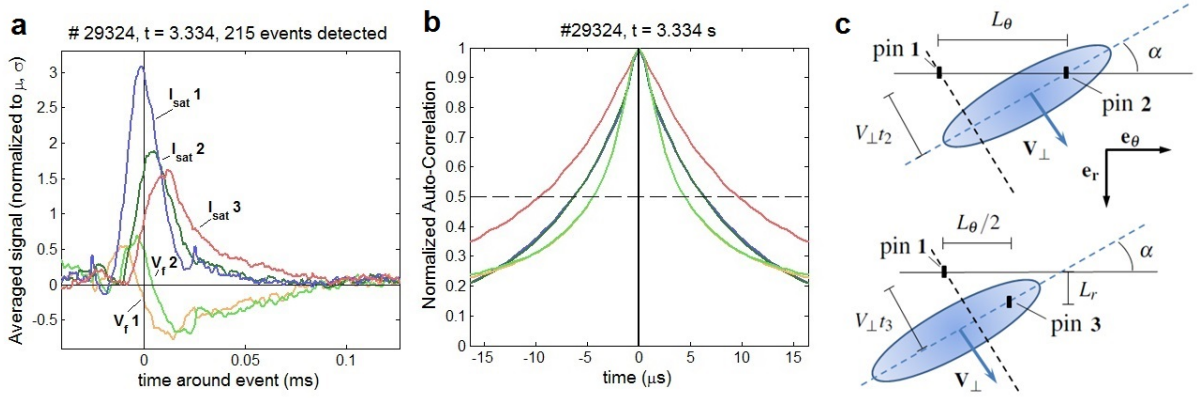

Figure 2: *Left, typical result of conditional averaging. Center, characteristic auto-correlation curves of all five signals. The 0.5 threshold (dashed line) defines auto-correlation times. Right, geometry of blob passage over pins 2 (t_2, upper) and 3 (t_3, lower).*

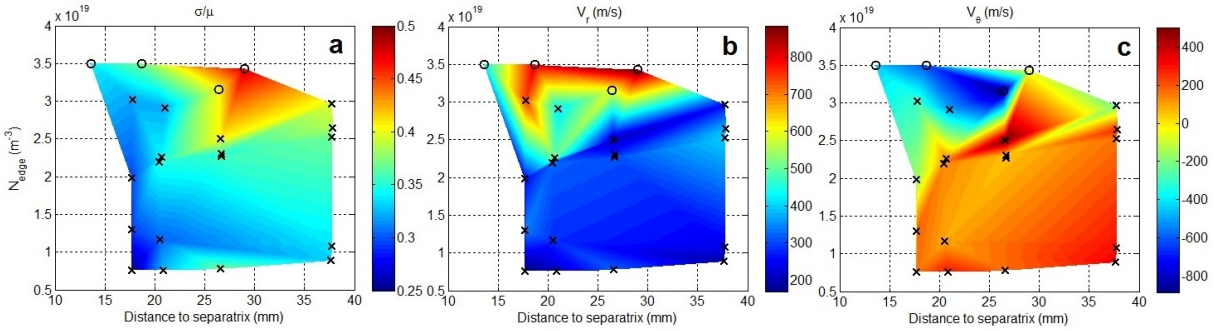

Figure 3: *Filament amplitude (std normalized with average value in the window, σ/μ), V_θ and V_r as a function of ΔR and $\bar{n}_e$. Each plunge is indicated by a black cross (plunges with 1 MW ECH are indicated as circles). Colors are linearly interpolated between points as a guide to the eye.*

As can be seen, there is a clear correlation between the structures recorded in the five signals, indicating that filaments traverse typically all pins. Besides conditional analysis, auto-correlation time of each signal (Δt_i, shown in the central plot of Figure 2) was obtained. The described conditional analysis yields the time of passage of the average filament over each pin, defined as $t_i = 1/T \int_T t S_i(t) dt$, where $S_i(t)$ is the signal coming from pin i. To analyze the propagation of the filament, a novel analysis technique is used: since the typical size of these structures is substantially larger than the separation of the pins, the usual cross-correlation analysis fails to include the shape and tilt angle of the structures. Instead, the cross-section of filaments is approximated as an ellipse with a tilt α with respect to the poloidal direction and t_i is defined as the time at which the pin crosses the major axis (see right plot of Figure 2). The passage over the reference pin is set arbitrarily as $t_1 = 0$. Since only two additional pins are available for this analysis, perpendicular velocity $V_\perp$ is also assumed to be aligned with the axis of symmetry of the filament (i.e., perpendicular to the major axis). Thus, combining the geometric information of Figure 2:

$$V_\perp = \left(\left[\frac{t_2}{L_\theta} \right]^2 + \left[\frac{2t_3 - t_2}{2L_r} \right]^2 \right)^{-\frac{1}{2}}, \quad \sin\alpha = \frac{t_2}{L_\theta} V_\perp. \tag{1}$$

Then, $V_\theta = V_\perp \sin\alpha$ and $V_r = V_\perp \cos\alpha$. Finally, the spatial size of the filament cross-section can be calculated as $\Delta x = V_\perp \Delta t_1$.

The effect of the density increase on the turbulence is displayed in Figure 3, where the results of the described analysis for each plunge are displayed as a function of ΔR and edge density (measured by interferometry) at those times. As can be seen, for $\bar{n}_e > 2.5 \cdot 10^{19}$ m^{-3} the increase of density yields higher filament amplitude in the far SOL (Plot a) and greater propagation speed towards the wall (Plot b). As well, some velocity shear appears in the poloidal direction (Plot c).

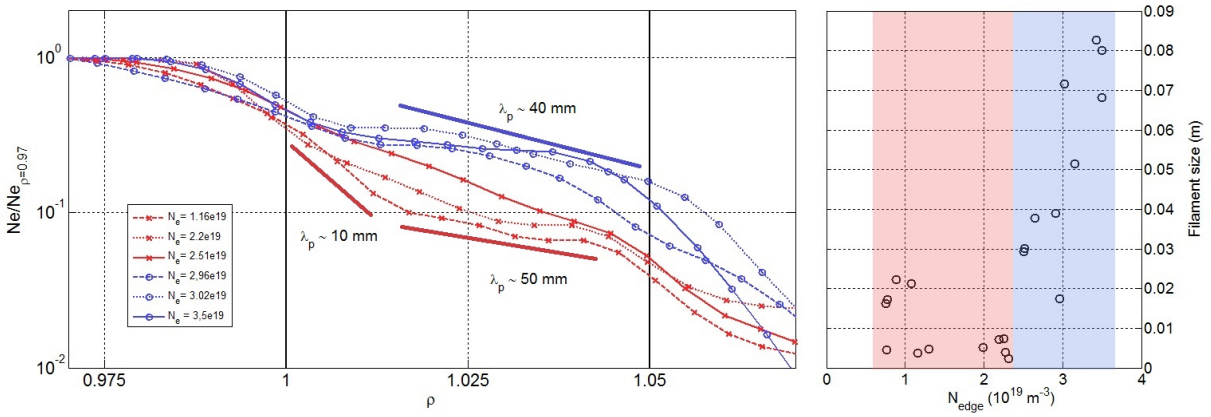

Figure 4: *Left, density profiles, as measured by the LiB, for several $\bar{n}_e$ values. The dashed line indicates the limiter shadow. Right, filament size as a function of $\bar{n}_e$.*

Interestingly, this regime change in the filaments seems to be followed by a change in the SOL transport: In Figure 4 left, the density profiles measured by the lithium beam during several plunges of increasing density are shown, normalized to the density value at the top of the profile ($\rho = 0.97$). As can be seen, for $\bar{n}_e > 2.5 \cdot 10^{19}$ m^{-3} (blue curves), the strong gradient in the near SOL disappears and the flat region originally only present in the far SOL extends almost to the separatrix. Finally, as can be seen in Figure 4 right, this change in transport regime coincides with a clear increase in the size of filaments (which would eventually become comparable to the width of the SOL).

These results are reminiscent of those observed in Alcator C-Mod[4] and seem to indicate a clear regime change both in the filament characteristics (most remarkably, filament size begins to increase linearly with $\bar{n}_e$) and the overall particle transport in the SOL, with the strong gradient region in the near SOL (typically associated to electron-channel parallel-dominated transport) disappearing, and the flat gradient of the far SOL (associated to advective perpendicular-dominated transport) extending almost to the separatrix and increasing perpendicular transport in this region by a factor $4-5$.

References

[1] S. I. Krasheninnikov, D. A. D´Ippolito and J. R. Myra, Journal of Plasma Physics, **74**, 679717 (2008)

[2] O. E. Garcia, N. H. Bian, and W. Fundamenski, Physics of Plasmas, **13**, 082309 (2006)

[3] J. R. Myra, D. A. Russell, and D. A. D´Ippolito, Physics of Plasmas, **13**, 112502 (2006)

[4] B. LaBombard, R. L. Boivin, M. Greenwald, J. Hughes et al., Physics of Plasmas, **8**, 2107 (2001)

[5] O. E. Garcia, N. H. Bian, and W. Fundamenski, Physics of Plasmas, **13**, 082309 (2006)

[6] B. Nold, G. D. Conway, T. Happel, H. W. Müller, Plasma Phys. Control. Fusion **52**, 065005 (2010)